Article:
Dufferwiel, S., Lyons, T.P., Solnyshkov, D.D. et al. (9 more authors) (2017)
Valley-addressable polaritons in atomically thin semiconductors. Nature Photonics, 11. pp. 497-501. ISSN 1749-4885

https://doi.org/10.1038/nphoton.2017.125

Valley addressable polaritons in atomically thin semiconductors

S. Dufferwiel,[1,*] T. P. Lyons,[1] D. D. Solnyshkov,[2] A. A. P. Trichet,[3] F. Withers,[4,5] S. Schwarz,[1] G. Malpuech,[2] J. M. Smith,[3] K. S. Novoselov,[4] M. S. Skolnick,[1] D. N. Krizhanovskii,[1] and A. I. Tartakovskii[1,†]

[1] *Department of Physics and Astronomy, University of Sheffield, Sheffield S3 7RH, UK*
[2] *Institut Pascal, University Clermont Auvergne and CNRS, 24 Avenue Blaise Pascal, 63178 Aubiere Cedex, France*
[3] *Department of Materials, University of Oxford, Parks Road, Oxford OX1 3PH, UK*
[4] *School of Physics and Astronomy, University of Manchester, Manchester M13 9PL, UK*
[5] *Centre for Graphene Science, CEMPS, University of Exeter, Exeter, EX4 4QF, UK*

(Dated: August 9, 2017)

The locking of the electron spin to the valley degree of freedom in transition metal dichalcogenide (TMD) monolayers has seen them emerge as a promising platform in valleytronics [1, 2]. When embedded in optical microcavities the large oscillator strengths of excitonic transitions in TMDs allow the formation of polaritons which are part-light part-matter quasiparticles [3–7]. Here, we report that polaritons in $MoSe_2$ show an efficient retention of the valley pseudospin contrasting them with excitons and trions in this material. We find that the degree of the valley pseudospin retention is dependent on the photon, exciton and trion fractions in the polariton states. This allows us to conclude that in the polaritonic regime, cavity-modified exciton relaxation inhibits loss of the valley pseudospin. The valley addressable exciton-trion-polaritons presented here offer robust valley polarised states with the potential for valleytronic devices based upon TMDs embedded in photonic structures and valley-dependent nonlinear polariton-polariton interactions.

Single layers of transition metal dichalcogenides (TMDs) are two-dimensional (2D) direct band-gap semiconductors which exhibit pronounced exciton resonances with binding energies of around 0.5 eV [8–10]. The monolayer nature of TMDs gives rise to strongly confined excitons with Bohr radii of around 1 nm and large oscillator strengths evident from optical absorption as strong as 15% [8]. By embedding TMD monolayers in optical microcavities this huge oscillator strength has allowed the realisation of the strong light-matter coupling regime and the formation of part-light part-matter polariton eigenstates [3–7]. Polaritonic states inherit properties such as a strong nonlinear interaction and low effective mass from the constituent exciton and photon components. In other material systems, this has led to the experimental realisation of a wealth of rich nonlinear phenomena such as Bose-Einstein condensation [11], superfluid-like behavior [12] and optical spin switching [13]. The observation of exciton-polaritons in TMDs creates new opportunities in engineering the polariton-polariton interaction [14, 15] in 2D materials. Moreover, TMD based polaritons are expected to inherit additional degrees of freedom of valley pseudospin and finite Berry curvature from their constituent excitons and trions which can be utilised in new valley-polaritonic implementations [16].

In this article we report on the valley addressability of polaritons in $MoSe_2$ monolayers embedded in tunable microcavities. We report clear valley polarisation of both exciton- and trion-polaritons which show a strong dependence of the polarisation degree on the cavity detuning. In the bare flake fast exciton depolarisation occurs due to the Maialle-Silva-Sham (MSS) mechanism [17–19]. We demonstrate that in the strong coupling regime this depolarisation mechanism can be overcome and robust valley-polarised polariton states with much higher polarisation degrees can be achieved. We support this conclusion using a dynamical model which reproduces the experimental data by incorporating cavity-modified relaxation of excitons to polariton branches which have long valley pseudospin relaxation times due to the reduced effect of exciton disorder scattering [20]. The demonstration of retention and control of valley polarisation and suppression of intervalley relaxation of $MoSe_2$ polaritons opens new avenues for the exploration of spin/valley dependent polariton-polariton interactions in TMD microcavity systems as well as the development of valleytronic devices based upon TMDs embedded in photonic structures.

The combination of time-reversal symmetry, strong spin-orbit coupling and the absence of crystal inversion symmetry in TMD monolayers leads to the coupling of spin and valley degrees of freedom [1, 2]. At both the conduction and valence band edges, the electron spin orientation is locked to the valley index allowing direct optical initialisation of the valley pseudospin in the non-equivalent K and K' valleys of the hexagonal Brillouin zone with σ^+/σ^- excitation respectively, as shown in Fig.1a and Fig.1b. The van der Waals (VDWs) heterostructure utilised in this study consists of a single monolayer of $MoSe_2$ encapsulated on both sides with thin films of hexagonal boron nitride (hBN) and placed on the surface of a planar distributed Bragg reflector (DBR). PL spectra under non-resonant σ^+ polarised excitation at 1.946 eV and 4.2 K for $MoSe_2$ are shown in Fig.1c. Two characteristic peaks are observed and ascribed to the neutral (X^0) and charged (X^-) exciton resonances. The polarisation degree, defined as

$\rho = (I_{co} - I_{cross})/(I_{co} + I_{cross})$ where I_{co} (I_{cross}) is the intensity component co-polarised (cross-polarised) relative to the excitation, is around 5% and 2% for the exciton and trion respectively, consistent with the low values previously reported in $MoSe_2$ [21].

A tunable microcavity is formed by introducing a top concave DBR into the optical path using nanopositioners and bringing the two DBRs to a total optical cavity length of around 2.9 μm [22]. The formed hemispherical cavity provides 3-dimensional photonic confinement, as shown in Fig.1d, leading to the formation of 0-dimensional Laguerre-Gaussian (LG) cavity modes [4]. The ground state longitudinal mode has a flat dispersion in momentum-space with an extent comparable to the inverse of the confined mode beam waist of ~ 1 μm. A clear anticrossing and the formation of polariton branches is observed in PL when the longitudinal mode is tuned through resonance with X^0 as shown in Fig.2a by reducing the DBR separation. Coupling to the first transverse cavity mode and the formation of polaritons (MPB2 and UPB2) is also present within the figure but all following discussion refers to the polariton branches formed due to coupling with the longitudinal mode. Fitting the polariton peak positions with a coupled oscillator model yields a Rabi splitting of 15.2 ± 0.1 meV for X^0. Analysis and fitting of the lineshape when close to resonance between the cavity and trion energies reveals the onset of strong coupling with a coupling strength of around 1.3 ± 0.1 meV as shown in Supplementary Fig.S1. The trion-polariton peaks are not fully resolved at resonance due to the cavity-trion Rabi splitting being comparable to the inhomogeneously broadened polariton linewidths. In an additional sample clear trion-polariton branches are resolved at resonance as discussed below. While the bare monolayer PL is dominated by trion emission, the trion-cavity coupling strength is much less than the exciton-cavity coupling strength. The oscillator strength, which is reflected in the Rabi splitting and not the PL intensity, is controlled by the position of the Fermi level [6, 23]. In our sample the Fermi level is determined by uncontrolled doping and is of a value such that the exciton oscillator strength is much larger than that of the trion. In the following discussion we take the peak below the trion as the lower polariton branch (LPB), the peak between the trion and exciton as the middle polariton branch (MPB) and the peak above the exciton as the upper polariton branch (UPB), as labelled in Fig.2a.

The retention of valley pseudospin of the polaritonic system was probed through excitation with non-resonant σ^+ circularly polarised light at 1.946 eV, close to a DBR reflectivity minimum. The same behaviour is observed under σ^- excitation. We perform the measurements in the low polariton density regime where the integrated intensity behaves linearly with pump power and where polariton-polariton interactions can be neglected (see Supplementary Fig.S2). Fig.2b shows the PL spectra at zero exciton-photon detuning for co- (black) and cross-polarised (red) collection, where clear retention of valley polarisation indicates an injected imbalance in the polariton valley populations. In-situ tunability of the cavity resonance allows the dependence of the polarisation degree on detuning to be probed through control of the mirror separation. The result for each polariton branch is plotted in Fig.2c where the cavity mode is tuned through resonance with X^- and X^0 as in Fig.2a, and the polarisation degree is calculated from the peak intensities of fitted spectra in co- and cross-polarised components. Spectra corresponding to a full range of detunings are shown in Supplementary Fig.S3 and S4. For the LPB we see a low polarisation degree when strongly negatively detuned and an abrupt increase to around 13% when close to resonance with X^-, before falling when positively detuned to the trion resonance. For detunings $\Delta > -20$ meV, coupling between the trion and higher order modes masks the polarisation degree of the trion-like LPB, so it is neglected in the following analysis. The MPB polarisation degree is initially low at negative detunings before rising to a maximum of 18% close to zero trion-cavity detuning, before dropping and increasing to around 15% when slightly negatively detuned from X^0, then falling to the bare exciton level at positive detunings. Finally the UPB shows an almost linear increase in polarisation degree with detuning, to a maximum value of around 17% at the maximum probed positive detuning of $\Delta = +25$ meV. For all polariton branches, the polarisation degree maxima are significantly enhanced in comparison to the bare exciton and trion resonances. Similar behaviour is measured for a second $MoSe_2$ sample with polarisation degrees of up to 20% as shown in Supplementary Fig.S6. In a third sample, trion-polariton peaks are resolved at resonance as shown in Fig.3a where a clear anticrossing between the cavity mode and trion state can be seen. The fitted peak positions are shown in Fig.3b where the extracted trion-cavity Rabi splitting is 4.4 ± 0.3 meV. Fig.3c shows polarisation resolved spectra of the trion-polariton branches at a trion-cavity detuning of +2.2 meV and an elevated temperature of 50 K where retention of valley polarisation is present in both polariton branches.

To describe the relaxation processes taking place in the system with both exciton and trion resonances coupled with a single cavity mode we consider the dynamical processes presented in Fig.4a. After photoexcitation, valley polarised carriers scatter to high in-plane wavevector (k-vector) excitonic states. The main valley pseudospin relaxation mechanism occurs here due to the Coulomb exchange interaction between the constituent valley electron and hole which leads to coupling of the K and K' valleys. The result is a splitting of the exciton states with the dipole moment parallel (L) and perpendicular (T) to the in-plane wavevector, with an energy splitting that is linearly dependent on k-vector outside the light cone [18, 19]. Circularly polarised light excites

a linear superposition of L and T excitons with a relative phase that corresponds to a state that initially has a well-defined valley polarisation. The LT-splitting can also be viewed in the pseudospin formalism as an effective magnetic field Ω_k that acts on the exciton valley pseudospin via the spin-valley coupling. The magnitude and direction of the effective field depend on the centre-of-mass momentum of the exciton as shown in the inset of Fig.4a [24]: the arrows indicate the orientation of the effective field for different orientations of the wavevector. For example, the positive and negative directions along the k_x axis both have a field pointing in the x-direction, because the longitudinal polarisation for antiparallel directions is the same. This is the reason explaining the double-winding texture of the effective field. Eigenstates have their pseudo-spin parallel and antiparallel to this field, which is fixing the relative phase between the wave functions in the two valleys. When the system is not in an eigenstate, the pseudospin precesses about the k-dependent effective field, which, combined with momentum scattering, is at the origin of the spin relaxation [17]. The scattering of the exciton k-vector due to disorder creates a randomly varying effective magnetic field leading to random spin precession and valley depolarisation, and is known as the Maialle-Silva-Sham (MSS) mechanism [17].

The high k-vector reservoir excitons relax along their dispersion to low k-vectors eventually forming MPB and LPB polaritons with relaxation rates W_{MPB} and W_{LPB}. Further valley pseudospin relaxation can then occur in the polariton branches before decay out of the cavity with a polariton radiative lifetime. The valley pseudospin relaxation time of the polaritons is much longer than that of the bare excitonic resonances since the spatial extent of the polariton wavefunction (1 μm) is much larger than the typical length scale of exciton disorder (10s of nm). This leads to significantly reduced polariton scattering by the disorder potential [20] and hence reduced valley depolarisation due to the MSS mechanism [17]. Assuming a thermal population of excitons in the reservoir and a polariton wavefunction size of ≈ 1 μm [25] and a linear dependence of the effective magnetic field with in-plane wavevector [18, 19] we estimate that the polariton spin relaxation time is around 20 times longer than the bare exciton (see Supplementary Note 1). In addition, polaritons are detuned from the exciton reservoir states (lower and middle polariton branches) or have a photonic component (upper polariton branch) so the scattering of polaritons back to the exciton reservoir is inhibited, leading to a non-zero net relaxation of high k-vector excitons to the polariton states. The UPB is a unique case as it is always degenerate with excitons at high k-vector due to the parabolic exciton dispersion. As such, the UPB can be populated by direct scattering of these excitons with a rate W_{UPB} and requiring a momentum change of around $\Delta k = 200\ \mu\text{m}^{-1}$. This momentum change corresponds to a localisation of excitons on the order of around 16 nm. The high polarisation degree of the UPB then reflects that of the degenerate high k-vector excitons.

For simplicity, in the model we neglect relaxation from the exciton reservoir to the trion reservoir due to trion formation and instead approximate that trion-polaritons are formed by direct relaxation from the exciton reservoir. This assumption is valid since the exciton relaxation rate from high k-vector to low k-vector occurs faster than the trion formation rate [26]. Thus only low k-vector trions are formed, for which the LT-splitting is small and hence spin relaxation is slow [19]. These trions then quickly relax to the trion-polariton branches. The resulting dynamical model and associated rate equations, which take into account detuning dependent relaxation, are presented in Supplementary Note 1. In particular, we show that the relaxation rates W_{MPB} and W_{LPB} are strongly dependent on the exciton-cavity detuning and can be related to the exciton, trion and photon components of the constituent polariton branches. We also show that W_{UPB} is proportional to the photonic component of the UPB state. The resultant polarisation dependence of the polariton branches as a function of detuning is shown in Fig.4b which accurately reproduces the experimental data. The main content of the theoretical model can be summarised as follows:

1. The valley pseudospin relaxation times used in Fig.4b are 0.15 ps and 1 ps for the bare exciton and trion respectively (see Supplementary Note 1). Depolarisation in $MoSe_2$ is due to interaction with disorder and localisation in the film where excitons undergo efficient (< 0.1 ps) scattering between low and high k-vectors leading to efficient depolarisation due to the MSS mechanism [17–19]. This leads to extrinsic valley depolarisation and the observed low polarisation degrees of the bare exciton and trion emission in $MoSe_2$. Intrinsic depolarisation due to phonon scattering of excitons will also contribute, but the effect of disorder scattering in current samples is dominant since the inhomogeneous broadening of 10-20 meV is much larger than the homogeneous linewidth of 1.6 meV [27].

2. The valley depolarisation times of the polariton states are an order of magnitude longer than the bare exciton and trion due to the reduced interaction with disorder [20]. Fast relaxation of excitons to the polariton branches before depolarisation then allows higher polarisation degrees to be observed in the polariton branches compared to the bare excitonic resonances.

In conclusion, we observe clear retention of valley polarisation in $MoSe_2$ exciton-polaritons and trion-polaritons. The strong dependence on the cavity detuning can be well described by a dynamical model that

incorporates modified relaxation and state lifetimes arising from strong coupling with the cavity mode. The spin-valley locking inherited by TMD polaritons from their exciton and trion components offers new avenues for valley-dependent polariton-polariton interactions where the populations of polaritons in K and K' valleys can be controlled with circularly polarised excitation. This allows the utilisation of the valley degree of freedom in polariton condensates [11], the optical spin hall effect [24, 28], optical spin switching [13] and polarisation bistabilities [29].

METHODS

Sample Preparation

The hBN-$MoSe_2$ stacks on DBR substrates were fabricated by mechanically exfoliated bulk $MoSe_2$ crystal onto a polymer double layer commonly used for dry transfer methods [30]. The $MoSe_2$ single layer flake was then used to lift, by van der Waals forces [30], a thin mechanically exfoliated hBN flake from a separate Si-SiO_2 substrate. The whole stack was then dropped down on the DBR substrate. The PMMA membrane along with the heterostructure stack was heated to 130 degrees to soften the PMMA followed by its removal in acetone then isoproponol. To preserve the $MoSe_2$ flake from environmental effects a second thin hBN flake was used to fully encapsulate the TMD. All bulk crystals including hBN were acquired from HQGraphene.

Optical Measurements

Optical measurements were performed with samples held in a helium bath cryostat system at a temperature of 4.2K. Top and bottom DBRs were attached to XYZ nanopositioners with additional goniometer stages allowing tilt control of the bottom DBR. Optical excitation of the bare monolayer was possible by removing the top DBR from the optical path. All μ-PL experiments were performed with continuous-wave (cw) excitation using a 638 nm laser diode, focused onto the sample with an achromatic lens. Polarisation resolved measurements were performed using a combination of linear polariser and a quarter waveplate in the excitation path, and quarter wave-plate, half wave-plate and linear polariser in the collection path. PL was collected by focusing onto a single mode fibre which was guided into a 0.75m spectrometer and a high sensitivity charge-coupled device.

Microcavity

The tunable microcavity with embedded TMD monolayer is formed using an external concave mirror to produce a zero-dimensional tunable cavity [25]. The formed cavity electric-field profile is shown in Supplementary Fig.S8 with the monolayer placed at an electric-field antinode, and nanopositioners are used to control the cavity spectral resonance energy. The nominal radius of curvature of the concave mirror is 20 μm leading to a beam waist on the planar mirror of around 1 μm [25].

DATA AVAILABILITY STATEMENT

The data that support the plots within this paper and other findings of this study are available from the corresponding author upon reasonable request.

MATERIALS AND CORRESPONDENCE

Correspondence and requests for materials should be addressed to A. Tartakovskii.

ACKNOWLEDGEMENTS

We thank the financial support of the Graphene Flagship under grant agreement 696656, the EPSRC grants EP/M012727/1 and EP/J007544/1, ERC Advanced Grant EXCIPOL No. 320570, and ITN Spin-NANO under grant agreement 676108. A. A. P. T., D. N. K and J. M. S. acknowledge support from the Leverhulme Trust. F. W. acknowledges support from the Royal Academy of Engineering and K. S. N. from the Royal Society, EPSRC, US Army Research Office and ERC Grant Hetero2D.

AUTHOR CONTRIBUTIONS

S.D and T. P. L carried out optical investigations. A. A. P. T. designed and fabricated the concave mirrors. F. W. fabricated the $MoSe_2$ samples. D. D. S. and G. M. carried out theoretical analysis. S. D. analysed the data and prepared the manuscript with contributions from all co-authors. J. M. S., K. N., M. S. S., D. N. K., and A. I. T. provided management of various aspects of the project. D. N. K proposed the idea of using an open-access microcavity system, developed by his group, for polariton studies with TMD monolayers. S. D and A. I. T. conceived the project. A. I. T oversaw the project.

* s.dufferwiel@sheffield.ac.uk
† a.tartakovskii@sheffield.ac.uk

[1] Xiao, D., Liu, G.-B., Feng, W., Xu, X., Yao, W., Coupled spin and valley physics in monolayers of MoS_2 and other group-VI dichalcogenides. *Phys. Rev. Lett.* **108**, 196802 (2012).
[2] Mak, K. F., He, K., Shan, J., Heinz, T. F. Control of valley polarization in monolayer MoS2 by optical helicity. *Nature Nanotech.* **7**, 494 (2012).
[3] Liu, X. *et al.* Strong lightmatter coupling in two-dimensional atomic crystals. *Nature Photon.* **9**, 30 (2015).
[4] Dufferwiel, S. *et al.* Excitonpolaritons in van der Waals heterostructures embedded in tunable microcavities. *Nature Commun.* **6**, 8579 (2015).
[5] Flatten, L. C. *et al.* Room-temperature exciton-polaritons with two-dimensional WS_2. *Scientific Reports* **6**, 33134 (2016).
[6] Sidler, M. *et al.* Fermi polaron-polaritons in charge-tunable atomically thin semiconductors. *Nature Phys.* **13**, 255 (2016).
[7] Lundt, N. *et al.* Room-temperature Tamm-plasmon exciton-polaritons with a WSe_2 monolayer. *Nature Commun.* **7**, 13328 (2016).
[8] Mak, K. F., Lee, C., Hone, J., Shan, J., Heinz, T. F. Atomically thin MoS_2: a new direct-gap semiconductor. *Phys. Rev. Lett.* **105**, 2 (2010).
[9] Berkelbach, T. C., Hybertsen, M. S., Reichman, D. R. Theory of neutral and charged excitons in monolayer transition metal dichalcogenides. *Phys. Rev. B* **88**, 045318 (2013).
[10] Ugeda, M. M. *et al.* Giant bandgap renormalization and excitonic effects in a monolayer transition metal dichalcogenide semiconductor. *Nature Mater.* **13**, 1091 (2014).
[11] Kasprzak, J. *et al.* Bose-Einstein condensation of exciton polaritons. *Nature* **443**, 409 (2006).
[12] Amo, A. *et al.* Superfluidity of polaritons in semiconductor microcavities. *Nature Phys.* **5**, 805 (2009).
[13] Amo, A. *et al.* Exciton-polariton spin switches. *Nature Photon.* **4**, 361 (2010).
[14] Marsault, F. *et al.* Realization of an all optical exciton-polariton router. *Appl. Phys. Lett.* **107**, 201115 (2015).
[15] Walker, P. M. *et al.* Ultra-low-power hybrid lightmatter solitons. *Nature Commun.* **6**, 8317 (2015).
[16] Yu, H., Cui, X., Xu, X., Yao, W. Valley excitons in two-dimensional semiconductors. *National Science Review* **2**, 57 (2014).
[17] Maialle, M. Z., de Andrada e Silva, E. A., Sham, L. J. Exciton spin dynamics in quantum wells. *Phys. Rev. B* **47**, 15776 (1993).
[18] Glazov, M. M. *et al.* Exciton fine structure and spin decoherence in monolayers of transition metal dichalcogenides. *Phys. Rev. B* **89**, 201302 (2014).
[19] Yu, H., Liu, G.-B., Gong, P., Xu, X., Yao, W. Dirac cones and Dirac saddle points of bright excitons in monolayer transition metal dichalcogenides. *Nature Commun.* **5**, 3876 (2014).
[20] Whittaker, D. M. *et al.* Motional narrowing in semiconductor microcavities. *Phys. Rev. Lett.* **77**, 4792 (1996).
[21] Wang, G. *et al.* Polarization and time-resolved photoluminescence spectroscopy of excitons in $MoSe_2$ monolayers. *Appl. Phys. Lett.* **106** 112101 (2015).
[22] Trichet, A. A. P. *et al.* Topographic control of open-access microcavities at the nanometer scale. *Opt. Express* **23**, 17205 (2015).
[23] Rapaport, R. *et al.* Negatively charged polaritons in a semiconductor microcavity. *Phys. Rev. B* **63**, 235310 (2001).
[24] Kavokin, A., Malpuech, G., Glazov, M. Optical Spin Hall Effect. *Phys. Rev. Lett.* **95**, 136601 (2005).
[25] Dufferwiel, S. *et al.* Strong exciton-photon coupling in open semiconductor microcavities. *Appl. Phys. Lett.* **104**, 192107 (2014).
[26] Godde, T. *et al.* Exciton and trion dynamics in atomically thin $MoSe_2$ and WSe_2: Effect of localization. *Phys. Rev. B* **94**, 165301 (2016).
[27] Moody, G. *et al.* Intrinsic homogeneous linewidth and broadening mechanisms of excitons in monolayer transition metal dichalcogenides. *Nature Commun.* **6**, 8315 (2015).
[28] Bleu, O., Solnyshkov, D., Malpuech, G. Optical valley hall effect based on transitional metal dichalcogenide cavity polaritons. arXiv:1611.02894 (2016).
[29] Sarkar, D. *et al.* Polarization bistability and resultant spin rings in semiconductor microcavities. *Phys. Rev. Lett.* **105**, 216402 (2010).
[30] Kretinin, A. V. *et al.* Electronic properties of graphene encapsulated with different two-dimensional atomic crystals. *Nano Lett.* **14**, 3270 (2014).

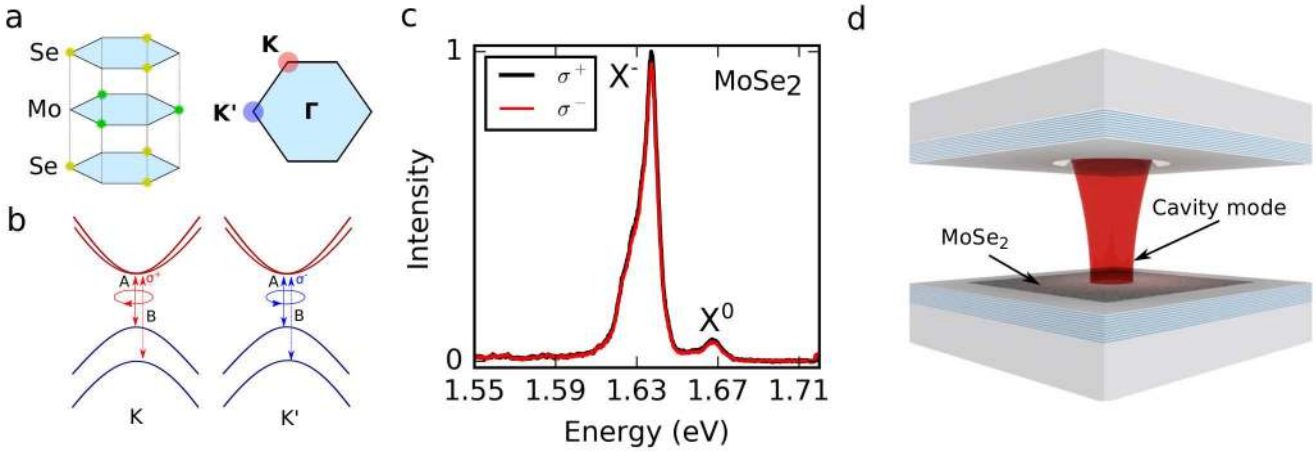

FIG. 1. **Spin-valley locking of excitons in $MoSe_2$.** **a** Illustration of the hexagonal lattice structure of $MoSe_2$. Optical band gaps are formed at the inequivalent K and K' valleys at the edges of the Brillouin zone. **b** Sketch of the valley dependent optical selection rules at the band edges. In the K (K') valley, the optical transitions couple to σ^+ (σ^-) polarised light. **c** PL spectra of $MoSe_2$ under σ^+ excitation showing A-exciton (X^0) and trion (X^-) emission in co- (black) and cross- (red) polarised detection. **d** Schematic of the 0-dimensional hemispherical microcavity with $MoSe_2$ active region.

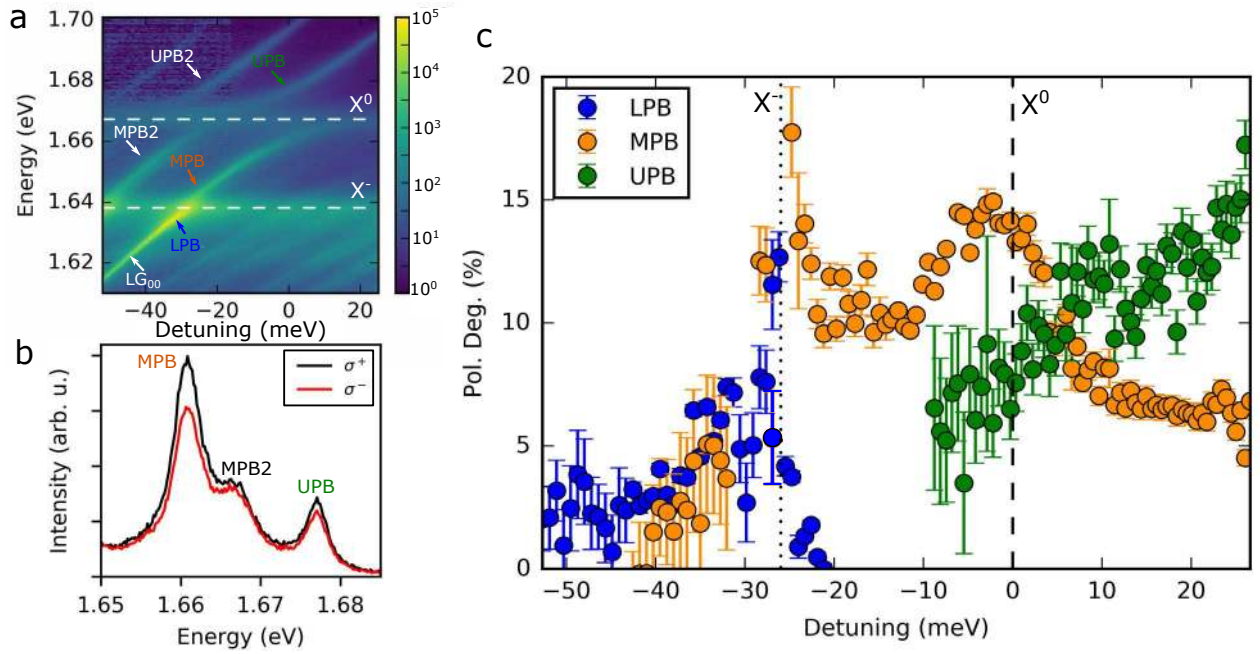

FIG. 2. **Valley addressable exciton-polaritons.** **a** Colourmap of PL spectra as a function of exciton-photon detuning ($\Delta = E_c - E_{X^0}$), where E_c and E_{X^0} are the tunable cavity and exciton energies, showing a clear anticrossing with X^0 with a Rabi splitting of 15.2 ± 0.1 meV. The onset of strong coupling is present for the trion with a coupling strength of 1.3 ± 0.1 meV. **b** PL spectra at zero exciton-photon detuning with σ^+ excitation. Clear retention of circular polarisation is seen to varying degrees in all peaks. **c** Circular polarisation degree of the polariton branches as a function of exciton-photon detuning. The vertical dashed and dotted lines correspond to zero exciton-cavity and zero trion-cavity detuning.

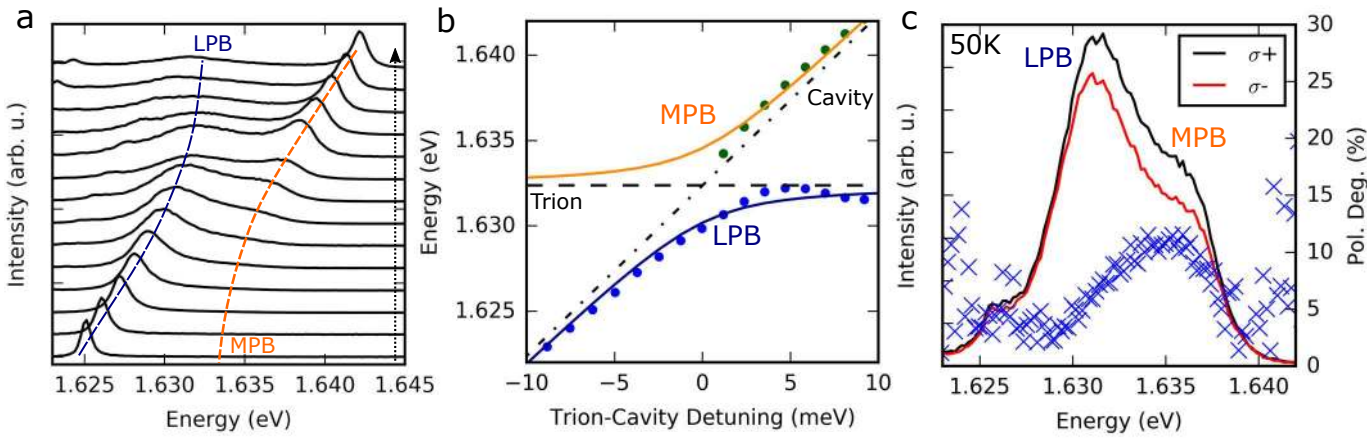

FIG. 3. **Valley-polarised trion-polaritons. a** Anticrossing between trion and cavity mode at 50 K for sample 3. The dashed line marks the direction of decreasing cavity length. **b** Coupled oscillator model fit to extracted peak positions as a function of trion-cavity detuning ($\Delta = E_c - E_{X^-}$), where E_c and E_{X^-} are the tunable cavity and trion energies. The trion-cavity Rabi splitting is 4.4 ± 0.3 meV. The anticrossing presented here is at $T = 50$ K as the increase in thermal energy is comparable to the trion-cavity Rabi splitting leading to a higher population of the MPB and a clearer resolution of the anticrossing. **c** Polarisation resolved PL spectra at trion-cavity detuning of +2.4 meV under σ^+ excitation at $T = 50$ K. Clear retention of circular polarisation is present in both trion-polariton branches as shown by the overlaid polarisation degree (blue crosses). The apparent increase in polarisation degree above 1.640 eV and below 1.625 eV is an artificial effect caused by the large data scatter from the low signal-to-noise in these regions.

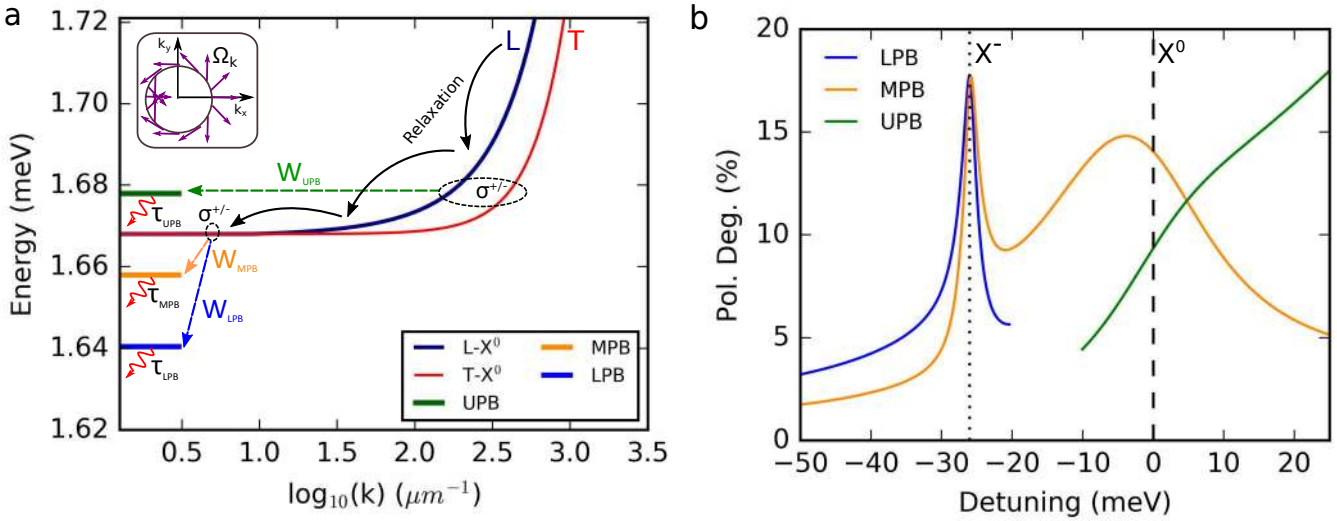

FIG. 4. **Cavity-modified relaxation dynamics. a** Dispersion of the exciton (dark blue and red lines) and polariton states (green/orange/blue filled lines). Valley-orbit coupling induces a linear splitting of the exciton dispersion into exciton states with the dipole moment parallel (L) and perpendicular (T) to the in-plane wavevector. The splitting is linear in k-vector outside of the light cone. The effective field texture due to the LT-splitting is shown in the inset. Dashed lines correspond to relaxation pathways of valley polarised excitons to polariton branches with a rate W_i where i =LPB, MPB, UPB. **b** Calculated circular polarisation degree of the three polariton branches as a function of detuning calculated from the model outlined in the text. The vertical dashed and dotted lines correspond to zero exciton-cavity and zero trion-cavity detuning.

Supplementary Information for "Valley addressable polaritons in atomically thin semiconductors"

S. Dufferwiel,[1,*] T. P. Lyons,[1] D. D. Solnyshkov,[2] A. A. P. Trichet,[3] F. Withers,[4] S. Schwarz,[1] G. Malpuech,[2] J. M. Smith,[3] K. S. Novoselov,[4] M. S. Skolnick,[1] D. N. Krizhanovskii,[1] and A. I. Tartakovskii[1,†]

[1]*Department of Physics and Astronomy, University of Sheffield, Sheffield S3 7RH, UK*

[2]*Institut Pascal, University Clermont Auvergne and CNRS, 24 Avenue Blaise Pascal, 63178 Aubiere Cedex, France*

[3]*Department of Materials, University of Oxford, Parks Road, Oxford OX1 3PH, UK*

[4]*School of Physics and Astronomy, University of Manchester, Manchester M13 9PL, UK*

(Dated: July 4, 2017)

SUPPLEMENTARY NOTE 1: THEORETICAL MODEL

The Boltzmann equations for the populations of the various states are given as:

$$\frac{dn_{X_\pm}}{dt} = P_+ - \frac{n_{X_\pm}}{\tau_X} - n_{X_\pm}\sum_{i=2}^{4} W_i \mp \frac{n_{X_+} - n_{X_-}}{\tau_{X_\pm}} \tag{S1}$$

$$\frac{dn_{i_\pm}}{dt} = W_i n_{X_\pm} - \frac{n_{i_\pm}}{\tau_i} \mp \frac{n_{i_+} - n_{i_-}}{\tau_{i_\pm}}, i = 2, 3, 4 \tag{S2}$$

Here $n_{X\pm}$ and $n_{i\pm}$ are the exciton and polariton populations in the K and K' valleys respectively, where i runs from 2 to 4 and denotes the UPB, MPB and LPB. $\tau_{i\pm}$ is the spin relaxation time of the polariton branch given below, and P_+ is the pumped valley-polarised population of particles. Solving these coupled rate equations in the steady state gives the solutions for the circular polarisation degrees of the exciton-polariton branches:

$$\rho_i = \frac{\tau_{i\pm}\tau_{X\pm}\left(1 + \tau_X \sum_{j=2}^{4} W_j\right)}{(2\tau_i + \tau_{i\pm})\left(\tau_{X\pm} + 2\tau_X + \tau_X\tau_{X\pm}\sum_{j=2}^{4} W_j\right)} \tag{S3}$$

For the exciton reservoir, the circular polarisation degree is given by:

$$\rho_X = \frac{\tau_{X\pm}\left(1 + \tau_X \sum_{i=2}^{4} W_i\right)}{\tau_{X\pm} + 2\tau_X + \tau_X\tau_{X\pm}\sum_{i=2}^{4} W_i} \tag{S4}$$

The circular polarisation degree for the polariton branches and for the system in general is given by the balance of the exciton spin relaxation time and exciton energy relaxation time (total scattering rate out of the exciton reservoir). If the average time the particle spends in the reservoir is longer than the spin relaxation time, the circular polarisation degree will be low.

The coupling of the exciton, trion, and photon modes is described by a coupled oscillator model, where the eigenenergies and the Hopfield coefficients are obtained from the matrix:

$$\begin{pmatrix} E_X & 0 & V_X \\ 0 & E_T & V_T \\ V_X & V_T & E_C \end{pmatrix} \tag{S5}$$

where $E_X = 1.667$ eV and $E_T = 1.639$ eV are the exciton and the trion energies and E_C is the photon energy, which varies from 1.720 to 1.580 eV. The Rabi splitting for the exciton is taken as $2V_X = 15.2$ meV, while for the trion we take $2V_T = 1.3$ meV. The corresponding eigenvectors give the exciton, trion, and photon fractions x_i, t_i, p_i. The polariton lifetime can be written as:

$$\frac{1}{\tau_i} = \frac{x_i}{\tau_{X0}} + \frac{t_i}{\tau_T} + \frac{p_i}{\tau_p} \tag{S6}$$

where τ_p, τ_{X0} and τ_T are the photon radiative lifetime, and exciton and trion non-radiative lifetimes respectively. Finally, for the polariton spin relaxation times we take the following dependence:

$$\frac{1}{\tau_{i\pm}} = \alpha\frac{x_i}{\tau_{X\pm}} + \beta\frac{t_i}{\tau_{T\pm}} + \frac{p_i}{\tau_{p\pm}} \tag{S7}$$

where we assume different valley pseudospin relaxation times for excitons, $\tau_{X\pm}$, and trions, $\tau_{T\pm}$. The coefficients α and β are required since the polariton spin relaxation due to the excitonic component is reduced in comparison to the bare flake exciton and trion. In the bare flake efficient scattering between low k (small LT-splitting) and high k (large LT-splitting) excitons occurs due to scattering on disorder or localisation giving rise to fast depolarisation. Since polaritons are formed from low-k excitons and scattering due to disorder is reduced for the polaritons we expect the contribution to the polariton depolarisation from the exciton component to be less than the bare exciton spin relaxation time. Assuming a thermal population of excitons in the reservoir and a polariton wavefunction ≈ 1 μm [S1] and a linear dependence of the effective magnetic field with in-plane wavevector [S2, S3] we estimate $\alpha \approx \beta \approx 0.05$. We also take into account spin relaxation of the photonic component, $\tau_{p\pm} = 15$ ps due to the finite TE-TM splitting of the ground state mode [S4] (see Supplementary Fig. S7).

The exciton-photon detuning affects the circular polarisation degree of the polariton emission via the excitonic (x_i) and trionic (t_i) fractions of the polariton states determining the scattering rates towards these states, while the lifetimes of the states are affected via their photonic fraction (p_i). The following dependences for the scattering rates to the middle and lower polariton branches (i = 3, 4), derived in Supplementary Note 2, are given by:

$$W_i = W_0(x_i + t_i)p_i \tag{S8}$$

where W_0 is the exciton energy relaxation rate. The scattering rates have to be proportional to the exciton fraction, and the exciton and trion are summed over, where we assume the presence of an extra electron does not change the relaxation mechanism. If the branch is completely excitonic it becomes degenerate with the exciton reservoir, and the scattering due to interaction with disorder towards the branch becomes balanced by an inverse scattering rate from the branch. The imbalance between the two scattering rates (forward and backward) $W_{X\to i} - W_{i\to X} \propto 1 - e^{-(E_X - E_i)/k_B T} \approx (E_X - E_i)/k_B T$ is therefore proportional to the photonic fraction in the first order approximation, hence $W_i \propto p_i$.

The UPB is a special case, as it is always resonant with some states of the exciton reservoir at high k-vectors. It is therefore possible for high momentum excitons to scatter directly to the photon-like UPB states due to interaction with disorder. The corresponding scattering rate is therefore only proportional to the photonic fraction, while the excitonic one does not play any role: i.e. the exchange between the exciton reservoir and the excitonic fraction of this branch is always strongly balanced. Moreover, since the excitons do not need to relax their energy, and need only to change their momentum, the characteristic time of this process is that of momentum relaxation (pseudospin relaxation), and not that of energy relaxation. Therefore, we assume that:

$$W_2 \propto p_i/\tau_{X\pm} \tag{S9}$$

Another consideration for the UPB is that the direct scattering from the reservoir not only drains it, shortening its lifetime and increasing the average polarisation degree, but also brings strongly polarised particles from higher energy states directly into the resonant polariton states. Since the spin precession rate is linearly proportional to the k-vector, we assume that the polarisation degree in the reservoir decreases linearly with energy, from 100% at the injection point ($E_X + 300$ meV) down to ρ_X at E_X. This polarisation degree can then decay in the UPB before being emitted out of the system, giving a renormalization $\tau_{2\pm}/(\tau_{2\pm} + \tau_2)$, derived in Supplementary Note 3. In order to reproduce the data the ratio of UPB polariton population coming from this direct scattering from the reservoir compared to indirect relaxation (Eq. S8) is required to be $1:1$. The excitonic, trionic and photonic frac-

tion used in the model to calculate the detuning dependent relaxation times, state lifetimes and spin relaxation times are shown in Fig. S9

We take the exciton and trion lifetimes as $\tau_{X0} = 5.3$ ps and $\tau_T = 12$ ps [S5] and assume that the non-radiative exciton reservoir lifetime is comparable to the exciton PL-lifetime ($\tau_X = 5.3$ ps). The photon lifetime measured from the cavity Q-factor at large negative detuning is $\tau_p = 1.3$ ps. Finally we take the exciton energy relaxation rate to be $W_0 = 1/0.15$ ps to reproduce the data; an upper limit of 1 ps can be justified from the resolution-limited rise time for $MoSe_2$ excitons in recent time resolved measurements [S6]. The polarisation dependence on detuning, shown in Fig. 4b of the main text, is well reproduced using exciton and trion valley relaxation times of $\tau_{X\pm} = 0.15$ ps and $\tau_{T\pm} = 1$ ps respectively.

The enhancement in polarisation degree of the lower and middle polariton branches relative to the bare monolayer case is due to cavity modified relaxation which allows $MoSe_2$ excitons to relax from the reservoir into polariton states quickly, inhibiting complete spin relaxation in the reservoir. In these polariton states, which are formed with excitons around $k \approx 0$, the exciton LT-splitting is small and hence the spin relaxation from the excitonic component of the polariton is around 20 times slower than the bare exciton(see Supplementary Note 1). This is much slower than the polariton lifetime, allowing lower and middle polariton branch particles to decay radiatively without further significant depolarisation, and with higher retention of valley pseudospin. When the photonic fraction of the polariton is high, relaxation into these polariton branches is less efficient causing larger accumulation of particles in the reservoir and hence low polarisation degree. At high exciton or trion fractions, scattering from the reservoir into these polariton branches is efficient, but the low photonic fraction, which determines the radiative decay and hence the imbalance between forward and backward scattering between polariton and reservoir states, leads to a longer time spent in the reservoir and hence low polarisation of emitted light. At intermediate detunings and roughly equal exciton and photon fractions a maximum in polarisation degree is seen which is a comprimise of efficient relaxation due to the exciton component and efficient radiative decay due to the photonic component. The high degree of valley polarisation in the UPB is due to direct scattering of high momentum excitons through interaction with disorder, populating the UPB with highly polarised particles which decay quickly due to their photonic component.

SUPPLEMENTARY NOTE 2: DERIVATION OF THE SCATTERING RATES

First, we would like to describe the scattering between the exciton reservoir (index X) and a polariton state (index 2). In general, the rate equations for the exchange between such states can be written as follows:

$$\begin{aligned} \frac{dn_X}{dt} &= -W_{X\to 2} n_X + W_{2\to X} n_2 \\ \frac{dn_2}{dt} &= +W_{X\to 2} n_X - W_{2\to X} n_2 \end{aligned} \tag{S10}$$

where we have omitted all other terms, e.g. lifetime, spin relaxation, etc. The scattering mechanism can be the exciton-phonon interaction or the exciton-exciton interaction: in presence of a thermalized exciton reservoir, both give the same dependence on the temperature and energy difference:

$$\begin{aligned} W_{X\to 2} &= W_0 x \\ W_{2\to X} &= W_0 x e^{-\frac{E_X - E_2}{k_B T}} \end{aligned} \tag{S11}$$

The excitonic fraction x of the polariton state appears in the scattering rate because only the exciton can efficiently interact with phonons, or the other excitons. The coefficient W_0 is the same for both scattering rates, but since in one case (scattering down) the energy (the phonon) is emitted and in the other (scattering up) – absorbed, the corresponding probability factors are different. Our goal is now to simplify these expressions, in order to obtain an analytical solution. Indeed, if the polariton branch is far below the reservoir, the scattering backwards from this branch to the reservoir is small and can be safely neglected. However, if this branch is close to the reservoir, this scattering is not negligible, and we need to introduce a correction to the scattering rate $W_{X\to 2}$ in order to take this into account. Indeed, in this case the scattering rates $W_{X\to 2}$ and $W_{2\to X}$ become comparable, as well as the populations, and so it is possible to write simply the difference of both terms:

$$W_{X\to 2} - W_{2\to X} = W_0 x \left(1 - e^{-\frac{E_X - E_2}{k_B T}}\right) \tag{S12}$$

which in the first order (when $(E_X - E_2) << k_B T$) can be written as

$$W_{X\to 2} - W_{2\to X} \approx W_0 x \frac{E_X - E_2}{k_B T} \tag{S13}$$

On the other hand, at strongly positive detunings $\Delta \gg V$ (V is one half of the Rabi splitting), both the photonic fraction p_2 and the relative energy of the polariton state with

respect to the exciton $(E_X - E_2)/\Delta$ scale as V^2/Δ^2, which allows to simplify the expression for the effective scattering rate by using the photonic fraction instead of the energy difference:

$$W^{eff}_{X\to 2} = W_{x\to 2} - W_{2\to X} \approx W_0 xp \tag{S14}$$

and the rate equation now contains a single term with a single effective scattering rate:

$$\begin{aligned} \tfrac{dn_X}{dt} &= -W^{eff}_{X\to 2} n_X \\ \tfrac{dn_2}{dt} &= +W^{eff}_{X\to 2} n_X \end{aligned} \tag{S15}$$

In Supplementary Note 1, we omit the index eff on the scattering rate.

The advantage of all these simplifications is that the final model with a reduced number of terms has a clear analytical solution for the polarisation degree.

SUPPLEMENTARY NOTE 3: SPECIAL CASE OF THE UPB

In the main text, we have discussed that one can assume an energy dependence of the polarisation degree within the reservoir: fully polarized particles are injected at high energy and they progressively lose their polarisation as they relax in energy. Therefore, if the UPB is resonant with some particular energy state within the reservoir, there will be an incoming scattering rate towards this UPB with a certain polarisation degree (higher than at the bottom of the exciton reservoir). These polarized polaritons of the UPB will then lose their polarisation within this branch, before being emitted out of the system. To obtain their final polarisation degree, let us consider the UPB as a separate system with a pumping P (which describes the scattering from the reservoir) carrying a polarisation degree ρ. The lifetime of the states of the UPB is τ_2 and the spin relaxation time $\tau_{2\pm}$. The rate equations for this reduced system can be written as follows:

$$\begin{aligned} \frac{dn_+}{dt} &= \frac{P(1+\rho)}{2} - \frac{n_+}{\tau_2} - \frac{n_+ - n_-}{2\tau_\pm} \\ \frac{dn_-}{dt} &= \frac{P(1-\rho)}{2} - \frac{n_-}{\tau_2} + \frac{n_+ - n_-}{2\tau_\pm} \end{aligned} \tag{S16}$$

The stationary solution of this system of equations is:

$$\begin{aligned} n_+ &= \frac{\tau_2(P\tau_2 + P\tau_\pm + P\rho\tau_\pm)}{2(\tau_2+\tau_\pm)} \\ n_+ &= \frac{\tau_2(P\tau_2 + P\tau_\pm - P\rho\tau_\pm)}{2(\tau_2+\tau_\pm)} \end{aligned} \tag{S17}$$

which gives a simple expression for the polarisation degree of the UPB:

$$\rho' = \frac{\rho\tau_\pm}{\tau_2 + \tau_\pm} \tag{S18}$$

used in the main text.

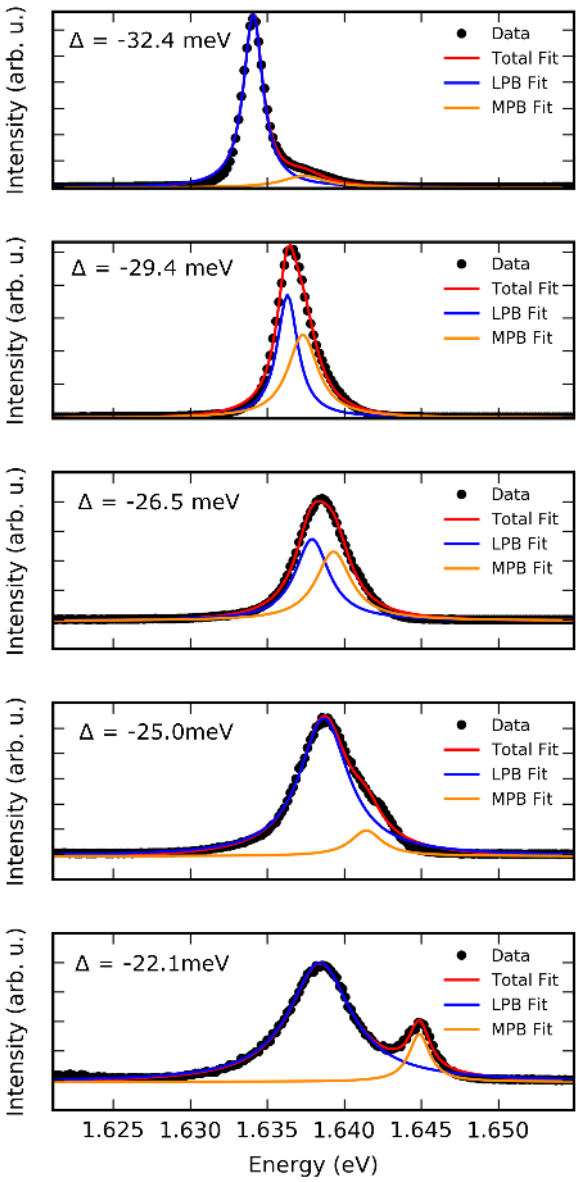

FIG. S1. Spectra as a function of detuning (Δ) when the cavity is tuned through resonance with the trion emission energy. The presence of two peaks when slightly detuned and a strong asymmetry of the peak at resonance indicates the onset of strong coupling. Here the Rabi splitting of 1.3 ± 0.1 meV is comparable to the inhomogeneously broadened polariton linewidths preventing the polariton branches from being fully resolved at resonance. The fits correspond to those used to extract the polarisation degree of the constituent polariton peaks.

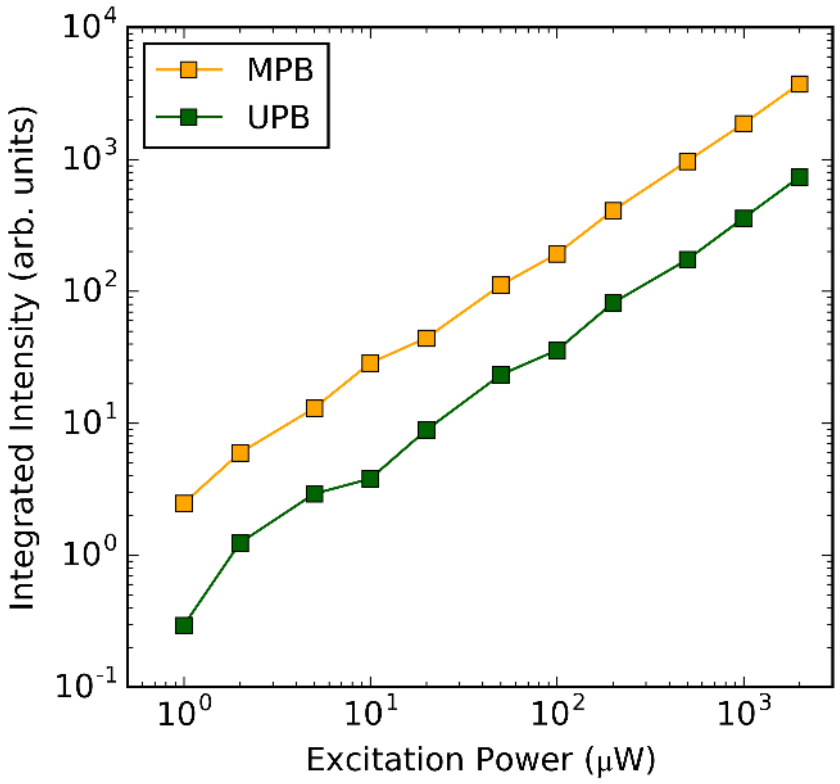

FIG. S2. Power dependence of integrated polariton emission at zero exciton-photon detuning. Measurements in the main manuscript were performed at 100 μW.

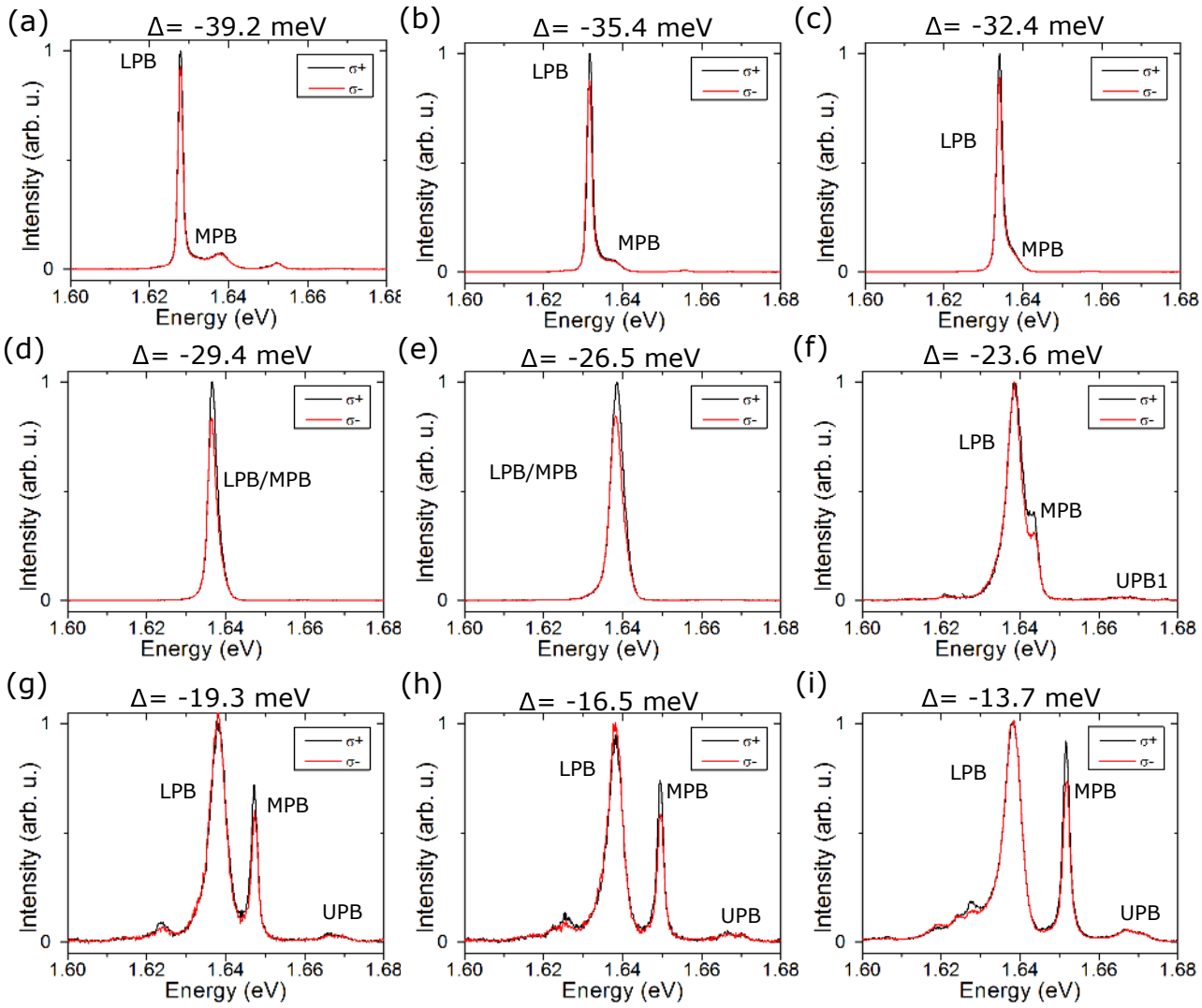

FIG. S3. Polarisation resolved spectra when the cavity mode is tuned through the $MoSe_2$ trion resonance (z-piezo voltages from 8.5V to 26V). Detunings (Δ) correspond to slices from in Figure 2b of main text.

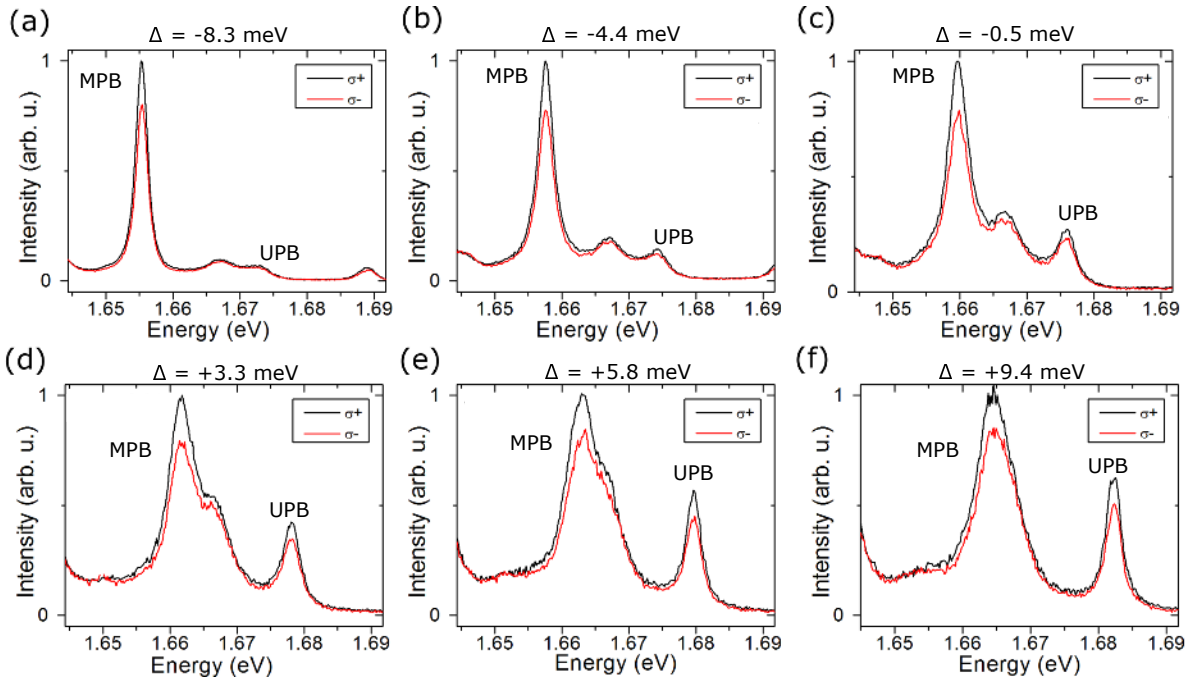

FIG. S4. Polarisation resolved spectra when the cavity mode is tuned through the $MoSe_2$ neutral exciton resonance. Detunings (Δ) correspond to slices from Fig. 2a of the main text. Polariton branches can clearly be resolved with a Rabi splitting of 15.2 meV which is significantly larger than the polariton linewidths. Varying degrees of retained valley polarisation are present for the polariton branches which strongly depend upon the exciton-photon detuning as discussed in the main text.

SUPPLEMENTARY NOTE 4: DATA FITTING PROCEDURE

Estimate of Rabi splitting and Polarisation Degree

Polariton branches are fitted with lorentzian functions in order to extract the peak positions to estimate the Rabi splitting. The Hamiltonian describing the coupling between the exciton, trion and photon is given by:

$$H = \begin{pmatrix} E_X & 0 & V_X \\ 0 & E_T & V_T \\ V_X & V_T & E_C \end{pmatrix} \tag{S19}$$

where E_X, E_T and E_C are the exciton, trion and cavity energies respectively. V_X and V_T are the exciton-photon and trion-photon coupling strengths.

The peak positions are obtained from a fit of multiple lorentzians to the various peaks using a non-linear least squares method. The peak positions are then simultaneously fitted with the analytical solution to the Eqn. S19 where all parameters are shared in the fitting procedure. The cavity mode energy is assumed to follow the relationship $E_c = y_0 + aV + bV^2$ where the coefficients a and b take into account the linear and nonlinear change in mirror separation as a function of applied piezo voltage (V). The resultant fit is shown in Fig. S5 where the fitted Rabi splittings for trion-cavity and exciton-cavity couplings are 1.0 ± 0.3 meV and 15.2 ± 0.1 meV respectively. The polarisation degree in Fig. 2 of the main text is calculated from the peak-intensity extracted from the fits of the co- and cross-polarized data. In Fig. 2 of the main text MPB data points at slight negative trion-cavity detuning have been discarded where fitting poorly reproduced the data. These correspond to fits which poorly reproduce the MPB intensity due to the order of magnitude difference in intensity between LPB and MPB at around -30 meV.

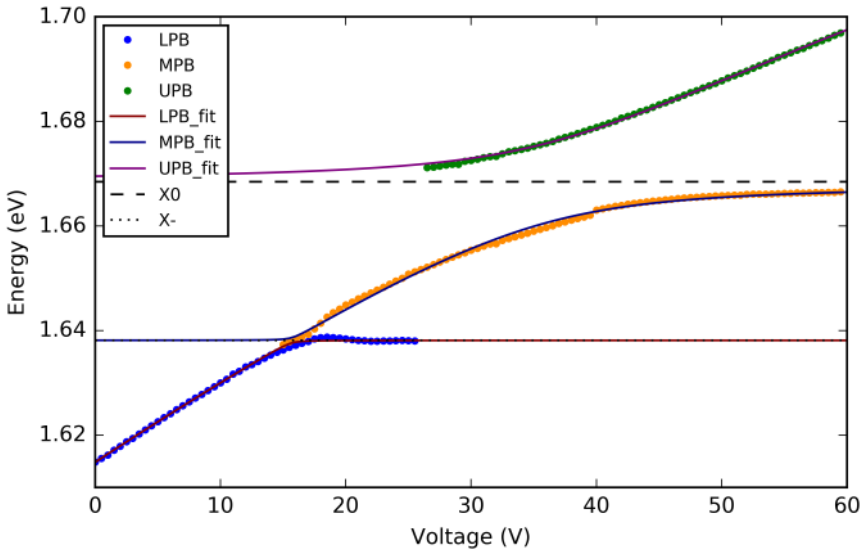

FIG. S5. Polariton peak energies fitted with 3-level coupled oscillator model.

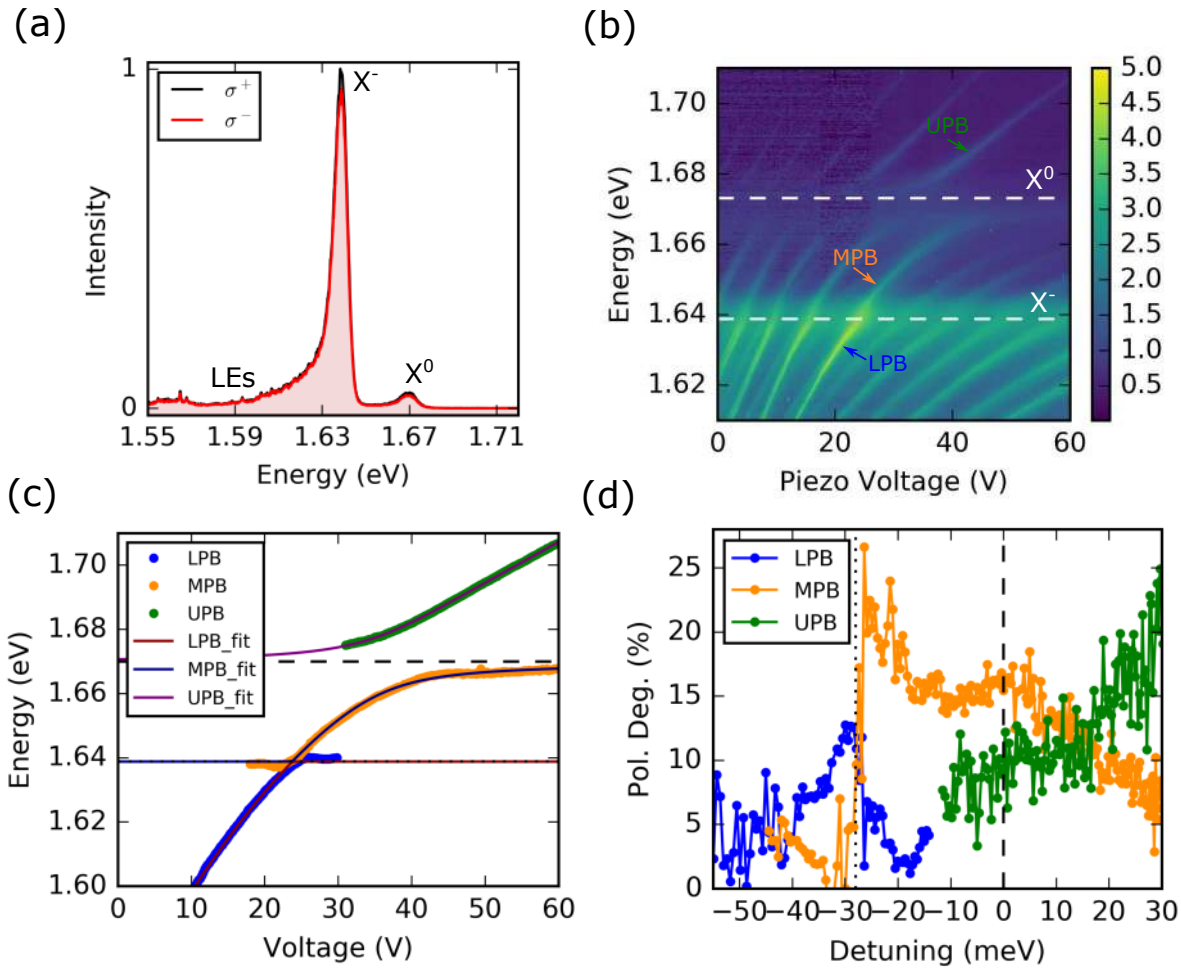

FIG. S6. Data for second sample consisting of hBN/MoSe2 heterostructure. (a) PL spectra of $MoSe_2$ under σ^+ excitation and co- (black) and cross- (black) polarized detection. The polarisation degree is 8% and 3% for the exciton and trion respecively. (b) Anticrossing between the ground state LG_{00} mode and the exciton energy. (c) Fitted peak positions giving neutral exciton Rabi splitting of 18.0 ± 0.1 meV and of 1.5 ± 0.2 meV for the trion. (d) Polarisation degree of the polariton branches as a function detuning.

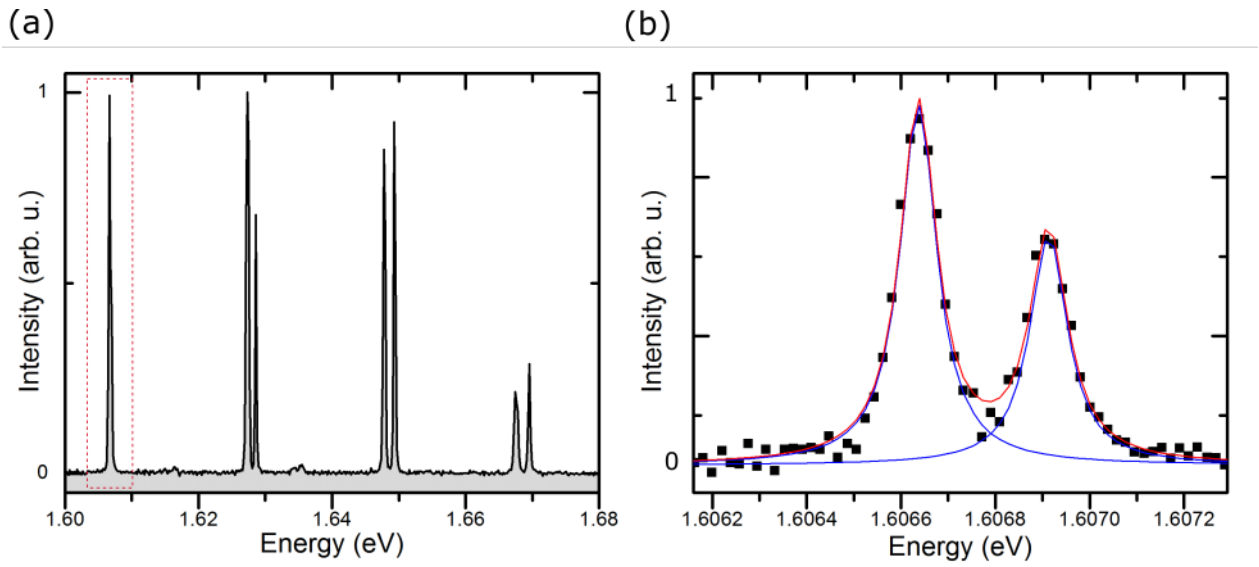

FIG. S7. (a) Cavity mode structure showing ground state (red box) and higher order transverse modes, which arise due to the harmonic like photonic confinement potential, in the weak coupling regime. (b) Spectrum of the TE-TM split ground state mode. The TE-TM splitting is 270 μeV.

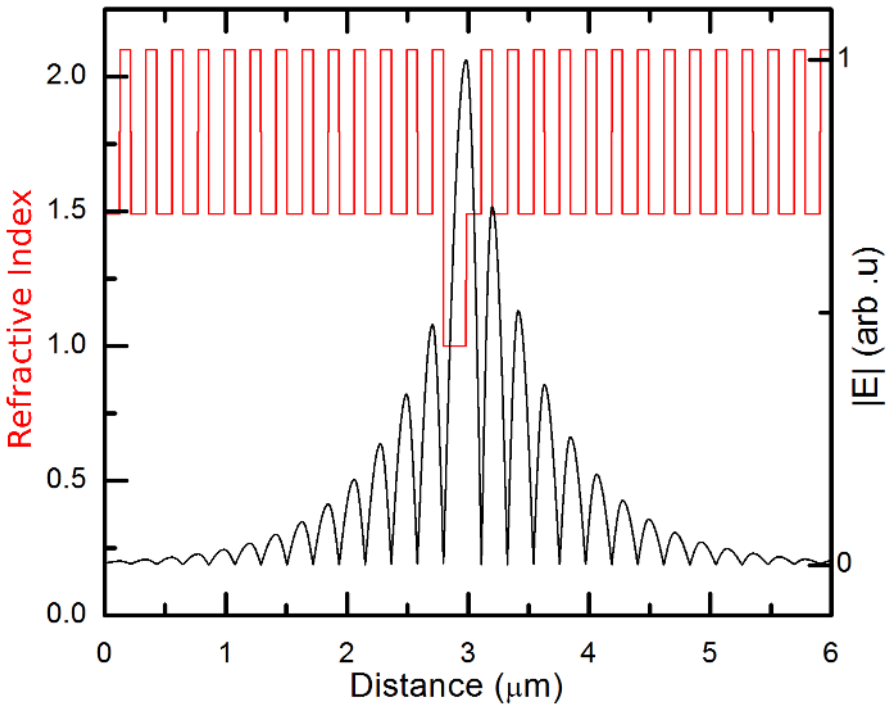

FIG. S8. Electric field distribution of microcavity calculated using the transfer matrix method (black trace) and the refractive index (red trace). The formed tunable microcavity consists of two dielectric DBRs seperated by a $q\lambda/4n$ gap, where q is the longitudinal mode index. The top concave DBR terminates with high index material giving a node at the surface while the bottom planar DBR terminates with low index giving an antinode. The TMD monolayer is placed at the surface of the bottom DBR at an electric-field antinode. The DBRs used in the main manuscript were 10 paired SiO_2/Nb_2O_5.

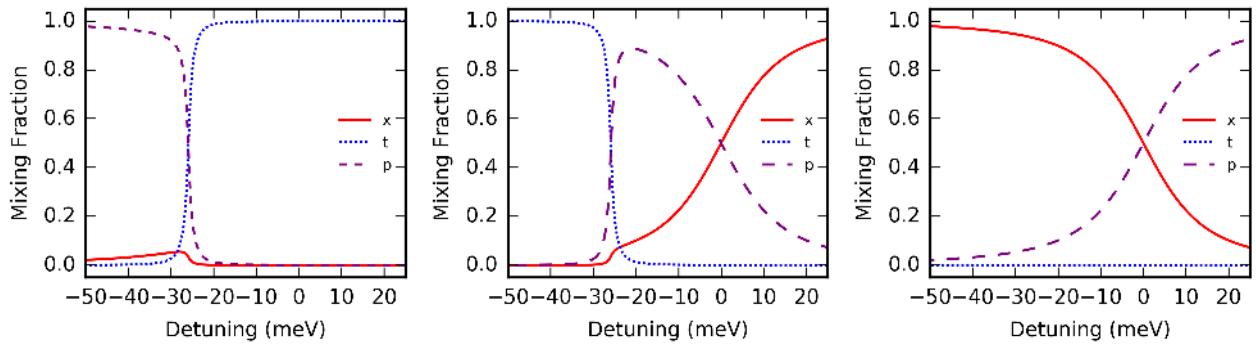

FIG. S9. Hopfield coefficients for the three polariton branches (a) LPB (b) MPB and (c) UPB used in the calculations of polarisation degree as a function of detuning shown in the main text.

* s.dufferwiel@sheffield.ac.uk

† a.tartakovski@sheffield.ac.uk

S1. S. Dufferwiel, F. Fras, A. Trichet, P. M. Walker, F. Li, L. Giriunas, M. N. Makhonin, L. R. Wilson, J. M. Smith, E. Clarke, M. S. Skolnick, and D. N. Krizhanovskii, Applied Physics Letters **104** (2014).

S2. M. M. Glazov, T. Amand, X. Marie, D. Lagarde, L. Bouet, and B. Urbaszek, Phys. Rev. B **89**, 201302 (2014).

S3. H. Yu, G.-B. Liu, P. Gong, X. Xu, and W. Yao, Nature Communications **5**, 3876 EP (2014).

S4. A. Kavokin, G. Malpuech, and M. Glazov, Phys. Rev. Lett. **95**, 136601 (2005).

S5. S. Dufferwiel, S. Schwarz, F. Withers, A. A. P. Trichet, F. Li, M. Sich, O. Del Pozo-Zamudio, C. Clark, A. Nalitov, D. D. Solnyshkov, G. Malpuech, K. S. Novoselov, J. M. Smith, M. S. Skolnick, D. N. Krizhanovskii, and A. I. Tartakovskii, Nature Communications **6** (2015).

S6. C. Robert, D. Lagarde, F. Cadiz, G. Wang, B. Lassagne, T. Amand, A. Balocchi, P. Renucci, S. Tongay, B. Urbaszek, and X. Marie, Phys. Rev. B **93**, 205423 (2016).